Electr Eng (2007) 90:87–93
DOI 10.1007/s00202-006-0055-x

ORIGINAL PAPER

Implementation of a closed loop sliding mode observer for speed sensorless control of an indirect field oriented induction motor drives

Nihat Inanc

Received: 8 May 2006 / Accepted: 24 November 2006 / Published online: 11 January 2007

Abstract A new sliding mode flux and speed observer is proposed for indirect field oriented induction motor drive system. The error between the actual and observed currents converges to zero, which guarantees the accuracy of the flux observer. The rotor speed and the rotor time constant are estimated based on the estimated stator currents and rotor flux. The estimated rotor time constant is used in slip calculation and observer structures. The estimated speed is used as feedback to the speed regulation. Simulation and experimental results of the speed control verify the validity of the proposed speed estimation algorithm.

Keywords Induction machine · Indirect field oriented control · Sliding mode observer · Sensorless control

1 Introduction

Induction motor control without mechanical sensor is becoming more attractive drive systems. Reliability and low level of maintenance are the salient advantages of the sensorless control. Various methods to implement the sensorless control can be summarized as; using voltage and current signals available from the drive system, through the carrier frequency signal injection or creating saliency by changing the machine rotor structure. Last two methods mentioned above suffer from the disadvantage that they need either extra hardware or special rotor manufacturing and therefore, cannot be used for an off-the-shelf induction machine. The much-preferred choice for sensorless control for an off-the-shelf machine is through flux and speed estimation using terminal quantities. Therefore, the focus of this paper is flux and speed estimation using the voltage and current signals only.

The two major techniques for high performance sensorless control of induction machine are slip frequency control [1] and field orientation control [2]. The slip frequency control has been documented to be more sensitive to the rotor resistance variation [3–5]. Many on-line identification schemes of the rotor time constant have been designed [6–8]. These methods have provided some improvement, but are quite complex because they either require more parameters or have hardware complications. Some fuzzy logic based techniques [9–11] have been proposed to overcome the detuning. However, these solutions are also very complex with respect to the software and require extensive calculation that put extra load on the processor.

In this paper, the proposed observer estimates the machine speed as well as the rotor time constant and therefore, overcomes the problems, caused by rotor resistance variations, inherited by the slip frequency control. The sliding mode flux observers for induction machine have been investigated [12–17]. However, most of the studied observer structures depend heavily on the machine parameters. In this paper, a new sliding mode flux observer structure is proposed such that the convergence of the observed flux is guaranteed by the convergence of the observed currents. Once the convergence of the observed flux is guaranteed, then the rotor speed and the rotor time constant are found through the equivalent control. The closed loop sliding mode observer presented in this paper has several advantages over the ones presented the estimated stator current

N. Inanc (✉)
Engineering Faculty, Electrical Engineering Department, Yuzuncu Yıl University, Zeve Campus, 65080 Van, Turkey
e-mail: ninanc@yahoo.com

error to estimate the rotor flux. To avoid using sensors on the machine, terminal quantities of the machine are used to estimate the fluxes and speed of the machine. In this case, the success in achieving the field orientation depends heavily on how well the rotor flux position is estimated. To solve this problem, different algorithms are proposed. These proposed algorithms are categorized in to two basic groups [18]. First one is 'the closed-loop observers' where the feedback correction is used along with the machine model itself to improve the estimation accuracy [19,20]. Second one is 'the open-loop observers' in a sense an on-line model of the machine, which do not use the feedback correction [21,22]. One of the main problems for both of those observer structures is the integration process inherited from the induction machine dynamics, and some work is based on cancellation strategies to avoid the integration effect. The other important problem is insufficient information about the machine parameters, which yield the estimation of some machine parameters along with the sensorless structure. In this study, a closed-loop sliding mode observer has been used and a low-pass filter (LPF) has been used to solve the integration effect. The cut-off frequency of the LPF has been chosen as 5 Hz.

2 IFO sensorless control structure

The slip frequency proposed sensorless control scheme is shown in Fig. 1 In this drive system, the inner feedback loop performs the synchronous current regulation. The current command i_{qs}^{e*} is produced by the outer speed control loop based on the command speed (ω_r^*) and the observed speed ($\hat{\omega}_r$). This speed regulation is conventionally done by using a PI controller [23].

The induction machine model is defined by the stator currents and rotor fluxes as state variables in rotor flux oriented stationary reference frame by the following equations:

$$\frac{\partial i_{ds}^s}{\partial t} = \beta \frac{1}{T_r}\lambda_{dr}^s + \beta\omega_r\lambda_{qr}^s - k_1 i_{ds}^s + k_2 V_{ds}^s \quad (1)$$

$$\frac{\partial i_{qs}^s}{\partial t} = \beta \frac{1}{T_r}\lambda_{qr}^s - \beta\omega_r\lambda_{dr}^s - k_1 i_{qs}^s + k_2 V_{qs}^s \quad (2)$$

$$\frac{\partial \lambda_{dr}^s}{\partial t} = -\frac{1}{T_r}\lambda_{dr}^s - \omega_r\lambda_{qr}^s + \frac{L_m}{T_r} i_{ds}^s \quad (3)$$

$$\frac{\partial \lambda_{qr}^s}{\partial t} = -\frac{1}{T_r}\lambda_{qr}^s + \omega_r\lambda_{dr}^s + \frac{L_m}{T_r} i_{qs}^s \quad (4)$$

where

$$\sigma = 1 - \frac{L_m^2}{L_s L_r}, \quad T_r = L_r/R_r, \quad k_2 = \frac{1}{\sigma L_s}$$

$$\beta = \frac{k_2 L_m}{L_r}, \quad k_1 = k_2\left(R_s + \frac{L_m^2}{L_r T_r}\right)$$

T_r is the rotor time constant, ω_r is the electrical rotor speed, subscripts d and q are used for d-axis and q-axis components and superscript s represents stationary reference frame.

3 Sliding mode current and flux observers design

The proposed speed and rotor time constant estimation structure is based on sliding mode current and flux observers. Ensuring the convergence of the current observer, the equivalent control is produced. Then, it is used in the flux observation to produce fluxes along the d and q axes. Once the flux values are found, then the rotor speed and rotor time constant are estimated by using observed fluxes. For clarity (1–4) can be written as

$$\begin{bmatrix} \frac{\partial i_{ds}^s}{\partial t} \\ \frac{\partial i_{qs}^s}{\partial t} \end{bmatrix} = \beta \begin{bmatrix} \frac{1}{T_r} & \omega_r \\ -\omega_r & \frac{1}{T_r} \end{bmatrix} \begin{bmatrix} \lambda_{dr}^s \\ \lambda_{qr}^s \end{bmatrix} - k_1 \begin{bmatrix} i_{ds}^s \\ i_{qs}^s \end{bmatrix} + k_2 \begin{bmatrix} V_{ds}^s \\ V_{qs}^s \end{bmatrix} \quad (5)$$

$$\begin{bmatrix} \frac{\partial \lambda_{dr}^s}{\partial t} \\ \frac{\partial \lambda_{qr}^s}{\partial t} \end{bmatrix} = \begin{bmatrix} -\frac{1}{T_r} & -\omega_r \\ \omega_r & -\frac{1}{T_r} \end{bmatrix} \begin{bmatrix} \lambda_{dr}^s \\ \lambda_{qr}^s \end{bmatrix} + \frac{L_m}{T_r} \begin{bmatrix} i_{ds}^s \\ i_{qs}^s \end{bmatrix}$$

Proposed current and flux observer structures are

$$\begin{bmatrix} \frac{\partial \hat{i}_{ds}^s}{\partial t} \\ \frac{\partial \hat{i}_{ds}^s}{\partial t} \end{bmatrix} = \beta \begin{bmatrix} \psi_{dr} \\ \psi_{qr} \end{bmatrix} - k_1 \begin{bmatrix} \hat{i}_{ds}^s \\ \hat{i}_{ds}^s \end{bmatrix} + k_2 \begin{bmatrix} V_{ds}^s \\ V_{ds}^s \end{bmatrix} \quad (6)$$

$$\begin{bmatrix} \frac{\partial \hat{\lambda}_{dr}^s}{\partial t} \\ \frac{\partial \hat{\lambda}_{qr}^s}{\partial t} \end{bmatrix} = \begin{bmatrix} -\frac{1}{\hat{T}_r} & -\hat{\omega}_r \\ \hat{\omega}_r & -\frac{1}{\hat{T}_r} \end{bmatrix} \begin{bmatrix} \hat{\lambda}_{dr}^s \\ \hat{\lambda}_{qr}^s \end{bmatrix} + \frac{L_m}{\hat{T}_r} \begin{bmatrix} i_{ds}^s \\ i_{qs}^s \end{bmatrix} \quad (7)$$

where $\hat{\lambda}_{dr}^s$ and $\hat{\lambda}_{qr}^s$ are the observed rotor flux components in stationary reference frame, $\hat{i}_{ds}^s$ and $\hat{i}_{qs}^s$ are the observed stator currents used for generating sliding mode. $\hat{\omega}_r, \hat{T}_r$ are the estimates of the rotor electrical speed and rotor time constant, respectively. The sliding functions Ψ_{dr} and Ψ_{qr} are defined as

$$\psi_{dr} = -u_{ds}^0 \text{sign}(s_{ds})$$
$$\psi_{qr} = -u_{qs}^0 \text{sign}(s_{qs})$$

where

$$s_{ds} = \hat{\text{i}}_{ds}^s - i_{ds}^s$$
$$s_{qs} = \hat{\text{i}}_{qs}^s - i_{qs}^s$$

and the sliding mode surface is defined as

$$s_n = \begin{bmatrix} s_{ds} & s_{qs} \end{bmatrix}^{\text{T}}$$

The existence condition for the sliding mode, ($\dot{s}_n s_n < 0$), will be

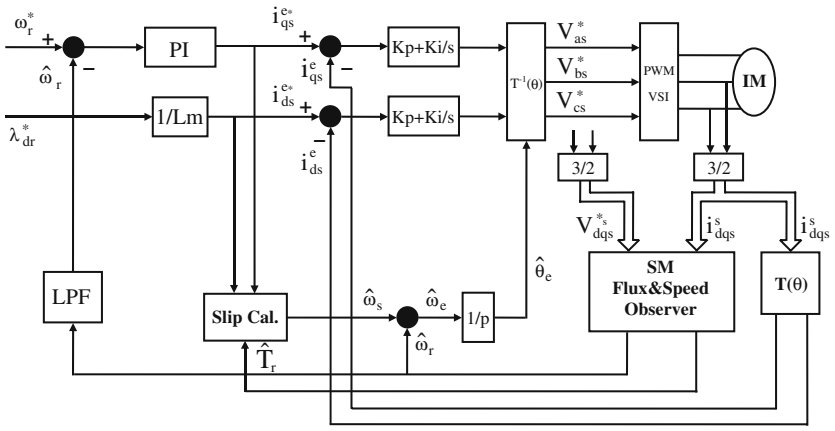

Fig. 1 Block diagram of the IFO closed-loop speed control with sliding mode observer structure

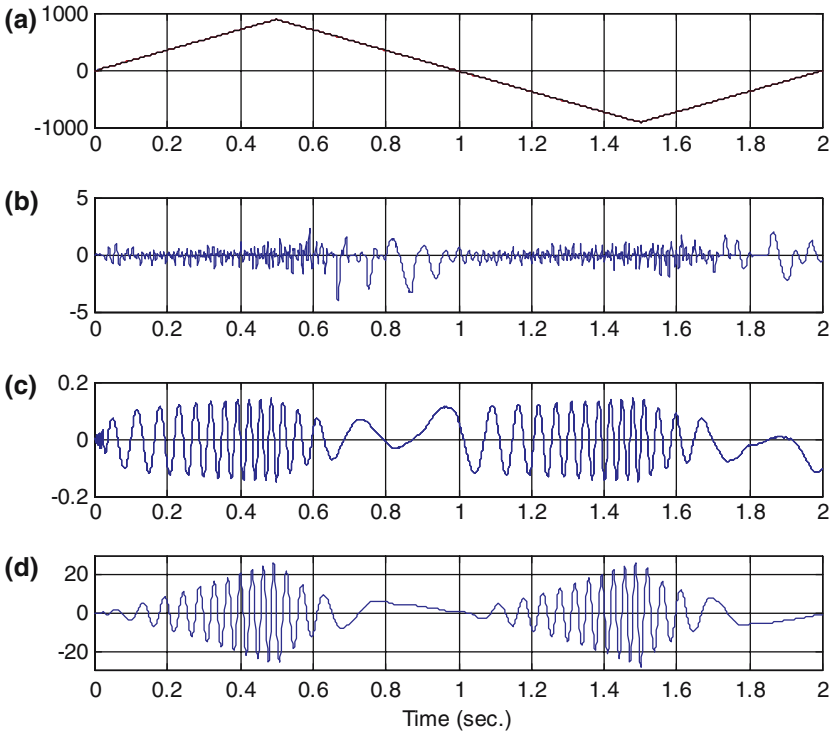

Fig. 2 Simulation results for a triangle speed command (900 rpm) without load: **a** observed and command speed tracking (rpm), **b** error between observed and command speed (rpm), **c** *d*-axis flux (Wb), and **d** designed *d*-axis sliding function

$$u^0_{ds}\rangle \left| -k_1 \bar{i}^s_{ds} - \beta \left(\frac{\lambda^s_{dr}}{T_r} + \omega_r \lambda^s_{qr} \right) \right|$$

$$u^0_{qs}\rangle \left| -k_1 \bar{i}^s_{qs} - \beta \left(\frac{\lambda^s_{qr}}{T_r} - \omega_r \lambda^s_{dr} \right) \right|$$

where $\bar{i}^s_{ds} = \hat{i}^s_{ds} - i^s_{ds}, \quad \bar{i}^s_{qs} = \hat{i}^s_{qs} - i^s_{qs}$

By selecting large values of u^0_{ds} and u^0_{qs}, found by the existence condition, the sliding mode ($s_n = 0$) will occur. Solving the $\dot{s}_n = 0$ for discontinuity term yields the continuous equivalent control. However, the resulting equivalent control will depend on machine parameters and be difficult to implement. Therefore, it is reasonable to assume that equivalent control is close to the slow component of the real control that can be derived by filtering out the high frequency component using a LPF. Implemented LPF structure is

$$\Psi^{eq}_{dqr} = \frac{1}{\mu s + 1} \Psi_{dqr}$$

where μ is the time constant of the filter and should be sufficiently small to preserve the slow component undistorted but large enough to eliminate the high frequency components. LPF output will be equal to the equivalent control on the sliding surface.

From the equivalent control concept [4] assuming the observed currents $\hat{i}^s_{qs}$ and $\hat{i}^s_{ds}$ match with actual currents i^s_{qs} and i^s_{ds} in the steady state, then using (5) and (6) the

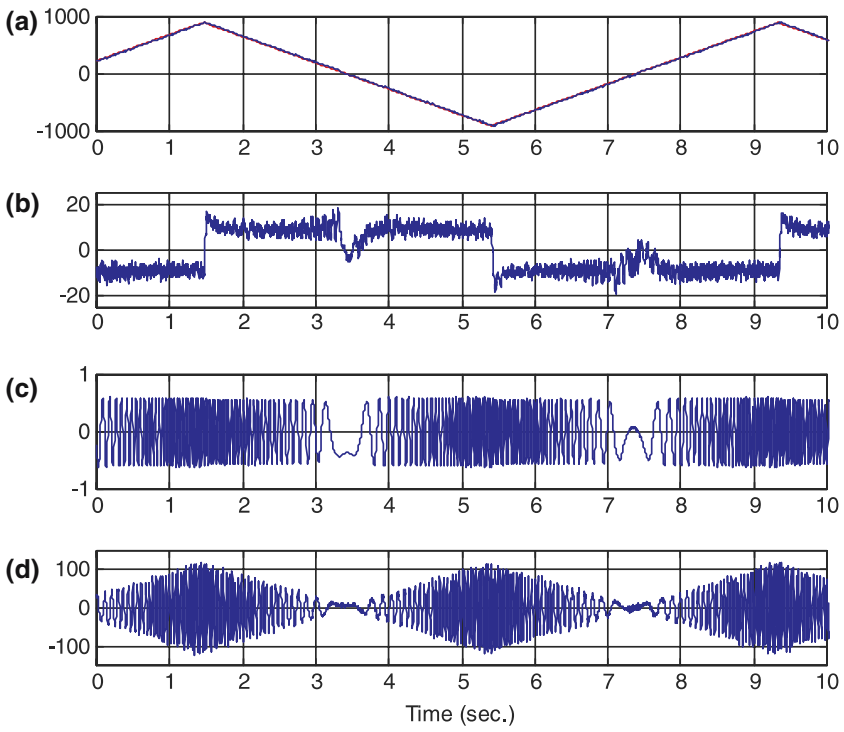

Fig. 3 Experimental results for a triangle speed command (900 rpm) without load: **a** observed and command speed tracking (rpm), **b** error between observed and command speed (rpm), **c** *d*-axis flux (Wb), and **d** designed *d*-axis sliding function

following equations can be derived:

$$\begin{bmatrix} \Psi_{dr}^{eq} \\ \Psi_{qr}^{eq} \end{bmatrix} = \begin{bmatrix} \frac{1}{\hat{T}_r} & \hat{\omega}_r \\ -\hat{\omega}_r & \frac{1}{\hat{T}_r} \end{bmatrix} \begin{bmatrix} \hat{\lambda}_{dr}^{s} \\ \hat{\lambda}_{qr}^{s} \end{bmatrix} \tag{8}$$

and using (7), (8) can be written as

$$\begin{bmatrix} \frac{\partial \hat{\lambda}_{dr}^{s}}{\partial t} \\ \frac{\partial \hat{\lambda}_{qr}^{s}}{\partial t} \end{bmatrix} = -\begin{bmatrix} \Psi_{dr}^{eq} \\ \Psi_{qr}^{eq} \end{bmatrix} + \frac{L_m}{\hat{T}_r} \begin{bmatrix} i_{ds}^{s} \\ i_{qs}^{s} \end{bmatrix}$$

from which the observed fluxes $\hat{\lambda}_{dr}^{s}$ and $\hat{\lambda}_{qr}^{s}$ can be found. Then using (8) speed and actual value of the rotor time constant can be found. To do this, (8) can be reorganized as:

$$\begin{bmatrix} \Psi_{dr}^{eq} \\ \Psi_{qr}^{eq} \end{bmatrix} = \begin{bmatrix} \hat{\lambda}_{dr}^{s} & \hat{\lambda}_{qr}^{s} \\ \hat{\lambda}_{qr}^{s} & -\hat{\lambda}_{dr}^{s} \end{bmatrix} \begin{bmatrix} \frac{1}{\hat{T}_r} \\ \hat{\omega}_r \end{bmatrix}$$

and

$$\begin{bmatrix} \frac{1}{\hat{T}_r} \\ \hat{\omega}_r \end{bmatrix} = \frac{1}{\left|\hat{\lambda}_r\right|} \begin{bmatrix} -\hat{\lambda}_{dr}^{s} & -\hat{\lambda}_{qr}^{s} \\ -\hat{\lambda}_{qr}^{s} & \hat{\lambda}_{dr}^{s} \end{bmatrix} \begin{bmatrix} \Psi_{dr}^{eq} \\ \Psi_{qr}^{eq} \end{bmatrix} \tag{9}$$

where

$$\left|\hat{\lambda}_r\right| = \left(-(\hat{\lambda}_{dr}^{s})^2 - (\hat{\lambda}_{qr}^{s})^2\right)$$

Finally, from (9), $\hat{\omega}_r$ and $\hat{T}_r$ are found as

$$\hat{\omega}_r = \frac{1}{\left|\hat{\lambda}_r\right|}\left(-\hat{\lambda}_{qr}^{s}\Psi_{dr}^{eq} + \hat{\lambda}_{dr}^{s}\Psi_{qr}^{eq}\right) \tag{10}$$

$$\hat{T}_r = \frac{-\left|\hat{\lambda}_r\right|}{\hat{\lambda}_{dr}^{s}\Psi_{dr}^{eq} + \hat{\lambda}_{qr}^{s}\Psi_{qr}^{eq}} \tag{11}$$

4 Simulation results

The block diagram of the indirect field oriented induction machine drive system with observer structure is shown in Fig. 1. The machine parameters used in this study are

220 V, 14.8 A, 5 Hp, $L_{ls} = L_{lr} = 1.9$ mH, $L_m = 41.2$ mH, 1,800 rpm, $R_s = 0.6\ \Omega$, $R_r = 0.412\ \Omega$, 4 poles

The validity of the observer structure is verified by the simulations, which are given in this section. Note that in the simulations, the observed speed is used as feedback in the closed loop and for the initial value of the rotor time constant, it is assumed that a rough estimation is known. In addition in all the figures actual and observed or estimated values and errors between them are presented.

Simulation results for a triangle speed command (900 rpm) without load are shown in Fig. 2. The command speed and observed speed are plotted in Fig. 2a. Figure 2b shows that the errors between command and

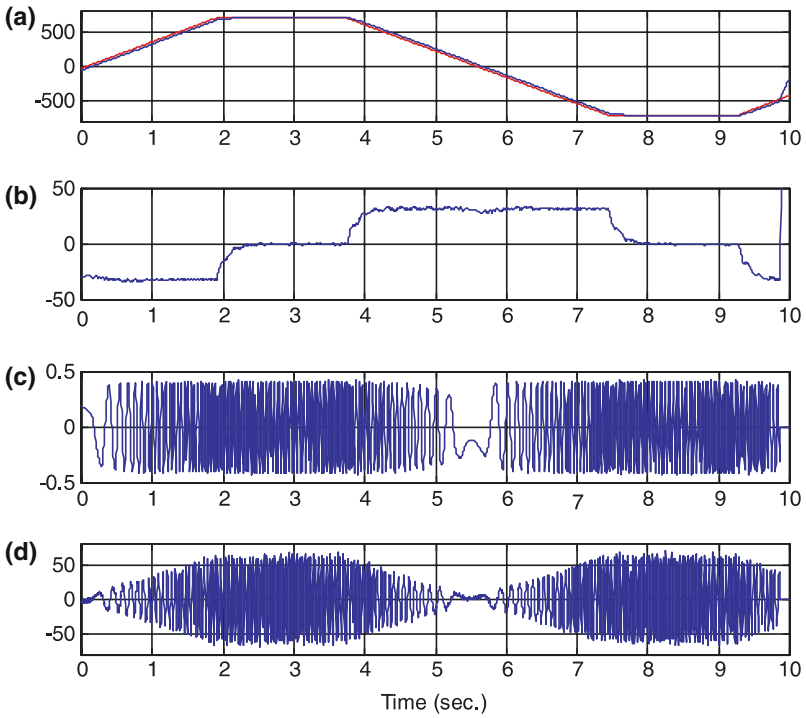

Fig. 4 Experimental results for a trapezoidal speed command (700 rpm) without load: **a** observed and command speed tracking (rpm), **b** error between observed and command speed (rpm), **c** *d*-axis flux (Wb), and **d** designed *d*-axis sliding function

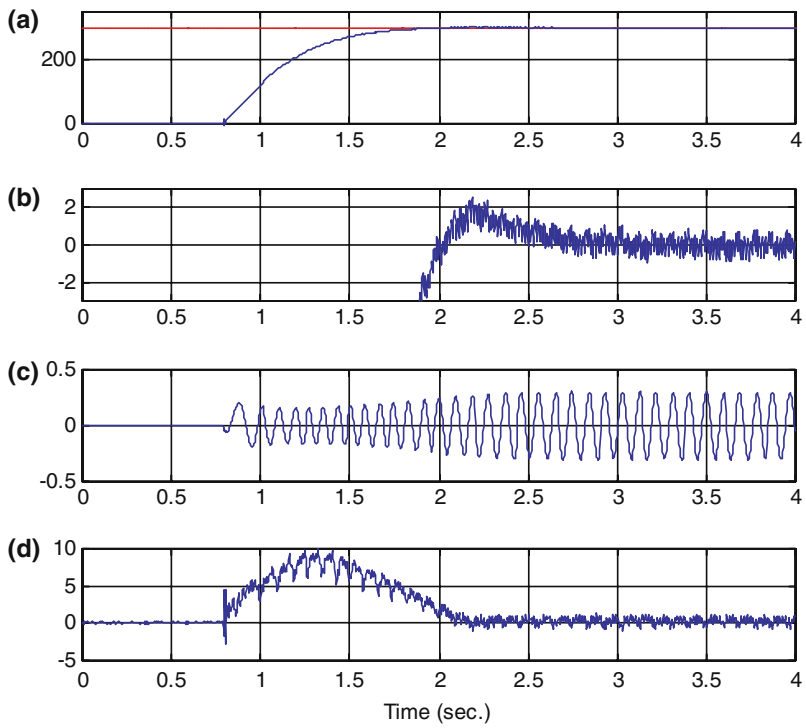

Fig. 5 Experimental results for a step speed command (300 rpm) without load: **a** observed and command speed tracking (rpm), **b** error between observed and command speed (rpm), **c** *d*-axis flux (Wb), and **d** designed *d*-axis sliding function

observed speeds are very small for triangular reference. Figure 2c shows *d*-axis flux. Figure 2d shows the sliding function, which is used to estimate the current and speed. When Figures for speed and current are examined, it is evident that the observers' performances are satisfactory since errors between actual and observed values are considerably small.

5 Experimental results

The laboratory setup consists of a 5 Hp cage rotor induction machine and a high performance Advance Controller for Electric Machines (ACE). For high speed performance, 900 rpm triangular and 700 rpm trapezoidal reference inputs are applied to the closed loop

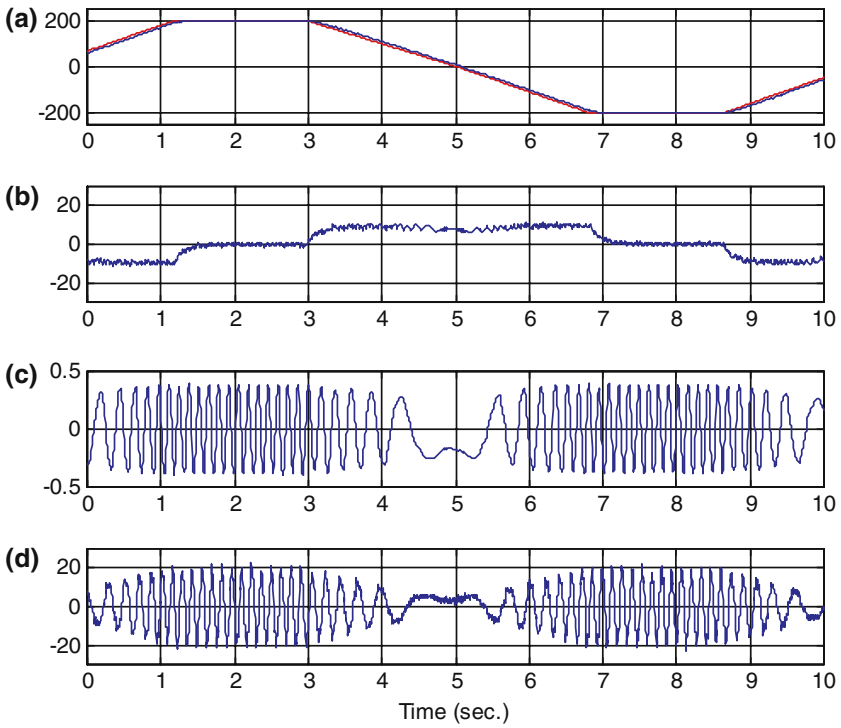

Fig. 6 Experimental results for a trapezoidal speed command (200 rpm) without load: **a** observed and command speed tracking (rpm), **b** error between observed and command speed (rpm), **c** *d*-axis flux (Wb), and **d** designed *d*-axis sliding function

system. In addition for the low speed performance, 300 rpm step and 200 rpm trapezoidal reference inputs are applied. In the following figures these results are presented.

To be able to prove the performance of the observers for the different speed conditions, several tests have been performed and the results are shown in Figures. The results shown in Figs. 3–6 prove that the proposed observer structure estimates the current and speed very well by using the designed sliding mode function.

Figure 3 shows that the observed speed is following the command speed, a 900 rpm triangular command. The maximum speed error is 18 rpm, i.e. 2%.

The speed error between the command and observed speed is 28 rpm (i.e. 4%) for a 700 rpm trapezoidal input without load as it can be seen from Fig. 4.

This maximum error is 2 rpm (i.e. 0.6%) for a 300 rpm step command in Fig. 5.

Figure 6 shows that the speed error between the command and observed speed is 10 rpm (i.e. 5%) for a 200 rpm trapezoidal input without load.

As can be seen from the experimental results, proposed algorithm is very robust and reliable for any speed condition. In the implementation, a LPF is used at the output of the speed estimator in the closed loop. The cut-off frequency of the LPF is chosen as 5 Hz in the implementation. Also, initially an approximate value of the rotor time constant is used in the closed loop. After rotor time constant estimator output converges to its actual value, the update process starts. Finally, command voltages are used instead of measured ones, and therefore only two current sensors are used in the overall system.

6 Conclusions

A new sliding mode flux, speed and current observers are proposed in this paper. The flux observer accuracy is guaranteed through the current observer. The error between the actual current and observed current converges to zero, which guarantees the accuracy of the flux observer. Under this condition, the rotor speed and rotor time constant are estimated. The rotor time constant update algorithm will overcome the problem of rotor resistance variation, normally needed for the slip frequency control. The proposed scheme is validated through the simulation and experimental results.

References

1. Ohtani T, Takada N, Tanaka K (1989) Vector control of induction motor without shaft encoder. In: Conference record of IEEE IAS annual meeting, pp 500–507
2. Tajima H, Hori Y (1993) Speed sensorless field-orientation control of the induction machine. IEEE Trans Ind Appl 29(1):175–180
3. Hori Y, Umeno T (1989) Implementation of robust flux observer based field orientation controller for induction

machine. In: Conference record of IEEE IAS annual meeting, pp 523–528
4. Nordin KB, Novotny DW (1985) The influence of motor parameter deviations in feed forward field orientation drive system. IEEE Trans Ind Appl IA-21:1009–1015
5. Krishnan R, Doran FC (1987) Study of parameter sensitivity in high-performance inverter-fed induction motor drive systems. IEEE Trans Ind Appl IA-23:623–635
6. Sugimoto H, Tamai S (1987) Secondary resistance identification of an induction motor applied model reference adaptive system and its characteristics. IEEE Trans Ind Appl IA-23:296–303
7. Matsuo T, Lipo TA (1985) A rotor parameter identification scheme for vector-controlled induction machine motor drives. IEEE Trans Ind Appl IA-21:624–632
8. Zai LC, Lipo TA (1987) An extensive Kalman filter approach to rotor time constant measurement in PWM induction machine drives. In: Conference record of IEEE IAS annual meeting, pp 177–183
9. Li Zhen, Longya Xu (1996) On-line fuzzy tuning of indirect field oriented induction machine drives. In: The Proceedings of IEEE APEC'96 conference, San Jose, California, March
10. Heber B, Xu L, Yifan Tang (1997) Fuzzy logic enhanced speed control of an indirect field-oriented induction machine drive. IEEE Trans Power Electron 12(5)
11. Li Zhen, Longya Xu (2000) Fuzzy learning enhanced speed control of an indirect field oriented induction machine drive. IEEE Trans Control Syst Technol 8(2)
12. Utkin VI (1993) Sliding mode control design principles and applications to electric drives. IEEE Trans Ind Electron 40(1):23–36
13. Inanc N (2002) A new sliding mode flux and current observer for direct field oriented induction motor drives. Elec Power Syst Res 63:113–118
14. Benchaib A, Rachid A, Auderzet E (1999) Sliding mode input-output linearization and field orientation for real-time control of induction motors. IEEE Trans Power Electron 14(1):3–13
15. Benchaib A, Rachid A, Auderzet E, Tadjine M (1999) Real-time sliding mode observer and control of an induction motor. IEEE Trans Ind Electron 46(1):128–137
16. Parasiliti F, Petrella R, Tursini M (1999) Adaptive sliding mode observer for speed sensorless control of induction motors. IEEE-IAS annual meeting conf record, pp 2277–2283
17. Lu H, Tai C (1999) Sensorless decoupling control of induction motors for high dynamic performance. IEEE Trans Ind Appl, pp 1565–1572
18. Jansen P, Lorenz R (1994) A physically insightful approach to the design and accuracy assessment of flux observers for field oriented induction machine drives. IEEE Trans Ind Appl 30(1):101–110
19. Yang G, Chin T (1993) Adaptive-speed identification scheme for a vector controlled speed sensorless inverter-induction motor drive. IEEE Trans Ind Appl 29(4):820–825
20. Kubota H, Matsuse K, Nakano T (1993) DSP based speed adaptive flux observer of induction motor. IEEE Trans Ind Appl 29(2):344–347
21. Hurst K, Habetler T, Griva G, Profumo F (1998) Zero speed tacholess IM torque control: simply a matter of stator voltage integration. IEEE Trans Ind Appl 34(4):790–794
22. Shin M, Hyun D, Cho S, Choe S (2000) An improved stator flux estimation for speed sensorless stator control of induction motors. IEEE Trans Power Electron 15(2):312–317
23. Derdiyok A, Guven MK, Rehman H, Inanc N, Xu L (2002) Design and implementation of a new sliding mode observer for speed sensorless control of induction machine. IEEE Trans Ind Electron 49:1177–1182